

An investigative study into the sensitivity of different partial discharge ϕ -q-n pattern resolution sizes on statistical neural network pattern classification

Mas'ud, Abdullahi Abubakar; Stewart, Brian G.; McMeekin, Scott G.

Published in:
Measurement

DOI:
[10.1016/j.measurement.2016.06.043](https://doi.org/10.1016/j.measurement.2016.06.043)

Publication date:
2016

Document Version
Author accepted manuscript

[Link to publication in ResearchOnline](#)

Citation for published version (Harvard):

Mas'ud, AA, Stewart, BG & McMeekin, SG 2016, 'An investigative study into the sensitivity of different partial discharge ϕ -q-n pattern resolution sizes on statistical neural network pattern classification', *Measurement*, vol. 92, pp. 497–507. <https://doi.org/10.1016/j.measurement.2016.06.043>

General rights

Copyright and moral rights for the publications made accessible in the public portal are retained by the authors and/or other copyright owners and it is a condition of accessing publications that users recognise and abide by the legal requirements associated with these rights.

Take down policy

If you believe that this document breaches copyright please view our takedown policy at <https://edshare.gcu.ac.uk/id/eprint/5179> for details of how to contact us.

An investigative study into the sensitivity of different partial discharge ϕ -q-n pattern resolution sizes on statistical neural network pattern classification

Abdullahi Abubakar Mas'ud^{1*}, Brian G. Stewart², Scott G. McMeekin²

Department of Electrical and Electronic Engineering Technology, Jubail Industrial College, KSA¹

School of Engineering and Built Environment, Glasgow Caledonian University, 70 Cowcaddeens Road, Glasgow, G4 0BA, UK²

Email address: masud_a@jic.edu.sa

Abstract

This paper investigates the sensitivity of statistical fingerprints to different phase resolution (PR) and amplitude bins (AB) sizes of partial discharge (PD) ϕ -q-n (phase-amplitude-number) patterns. In particular, this paper compares the capability of the ensemble neural network (ENN) and the single neural network (SNN) in recognizing and distinguishing different resolution sizes of ϕ -q-n discharge patterns. The training fingerprints for both the SNN and ENN comprise statistical fingerprints from different ϕ -q-n measurements. The result shows that there exists statistical distinction for different PR and AB sizes on some of the statistical fingerprints. Additionally, the ENN and SNN outputs change depending on training and testing with different PR and AB sizes. Furthermore, the ENN appears to be more sensitive in recognizing and discriminating the resolution changes when compared with the SNN. Finally, the results are assessed for practical implementation in the power industry and benefits to practitioners in the field are highlighted.

Keywords— classification, partial discharge and ensemble neural network, phase resolution and amplitude bin sizes.

29 Abbreviations

30	NN	neural networks
31	SNN	single neural network
32	ENN	ensemble neural network
33	PR	phase resolution
34	AB	amplitude resolution
35	PD	partial discharge
36	HV	high voltage
37	CI	confidence intervals
38	ϕ-q-n	phase-amplitude-number
39	IEC	international electrotechnical commission
40	$H_n(\phi)$	pulse count distribution
41	$H_{qn}(\phi)$	mean pulse-height
42	$H_n(q)$	amplitude-number
43	DEM	dynamically weighted ensemble network
44	DAN	dynamically averaged network
45	<i>sk</i>	skewness
46	<i>ku</i>	kurtosis
47	<i>Q</i>	discharge factor
48	<i>cc</i>	cross-correlation
49	<i>mcc</i>	modified cross-correlation
50	μ_S	average recognition rates of the SNN
51	μ_E	mean of the recognition efficiencies of the ENN
52	σ_S	variance of the recognition efficiencies of the SNN
53	σ_E	variance of the recognition efficiencies of the ENN
54	SEM	standard error of the mean
55	σ_{SM}	SEM of the recognition efficiencies of the SNN
56	σ_{EM}	SEM of the recognition efficiencies of the ENN

57

58

59 1. Introduction

60

61 Partial discharge (PD) measurements have been a vital index for evaluating electrical
62 insulation degradation under high voltage (HV) electrical stress. It is important to understand
63 the extent of insulation damage and the nature of an insulation fault through PD measurement
64 for reliable insulation assessment. PD is an electrical discharge that occurs within a localised
65 position of the electrical insulation when the insulation starts to degade [1] . If PD is detected,
66 it is also essential to recognize the nature and extent of the insulation defect, since each
67 particular PD fault has a distinct footprint pattern of discharge behaviour [2,3,4,5]. Over the
68 years, several techniques have been investigated for use in PD pattern recognition. These
69 include the neural network (NN)[1,6,7,8,9], fuzzy logic controllers [10], data mining
70 approaches [11], support vector machines[12], hidden markov models [13] and adaptive

resonance theory [14]. Such research has recorded successful recognition performance with recognition rates reaching as high as 90% for unseen PD fault examples. These successful rates were achieved through several feature extraction techniques when applied to acquire training and testing parameters for the pattern recognition tools. Statistical fingerprints from ϕ -q-n (phase-amplitude-number) patterns have been the most widely applied measures [1,15] for PD recognition because of their capability for well-defined PD pattern quantification. However, due to the complex nature of PD, coupled with degradation consequences, these statistical fingerprints may show different characteristics over different insulation degradation periods [16].

To improve the reliability and uniqueness of statistical fingerprints in being able to identify PD defects, Gulski and Krivda [1] made significant efforts by establishing 95% mean confidence intervals (CI) for statistical features for classes of several artificially created two electrode PD defects. The statistical mean error tolerances as obtained by Gulski and Krivda were based on fixed PR and AB sizes of the ϕ -q-n patterns and were determined from a series of measurements ranging from 4 to 23 separate ϕ -q-n patterns for the same type of PD fault. In this context, the research question is posed in relation to evaluating the sensitivity of statistical fingerprints for different ϕ -q-n PR and AB changes and how such variations in PR and AB could potentially influence classification outcomes when pattern recognition tools are applied. Moreover, further research is important because different measuring instruments may have different resolution settings for the ϕ -q-n pattern assessment and thus training data captured using a different set-up may vary from the actual measurement which may lead to an unreliable classification outcome.

In an attempt to address these situations, this paper aims at determining the sensitivity of statistical fingerprints as a function of PR and AB sizes of the ϕ -q-n patterns. For each statistical fingerprint defining a particular PD defect, statistical 95% mean error tolerances for different resolution sizes are compared, quantified and evaluated. To achieve this, a number of ϕ -q-n samples (ranging from 40 to 215) for different PD fault scenarios are considered. This is used to quantify the statistical behaviour as a function of PR or AB and provide potentially an improved classification tool since large datasets of the same PD sources are considered. Due to the success of the ensemble neural network (ENN) in classifying PD patterns [15], this paper extensively compares the ENN's capability with the single neural network (SNN) in classifying and discriminating different resolution sizes of the ϕ -q-n patterns over several statistical merit indicators. This is important to determine and compare

the statistical error bounds recognition rates of the SNN and ENN for different resolution sizes.

2. Experimental set-up and feature extraction

2.1 Artificially created PD faults

To obtain the PD samples for investigation, four different fault geometries were fabricated in a HV laboratory to simulate PD faults currently occurring in practice (see Fig. 1). These comprise corona in air and oil, surface discharges in air and oil, single voids and an electrode bounded cavity. The corona discharge model is a point-plane arrangement. A needle of length 3 cm and tip radius of approximately 10 μm is connected to the HV, while an electrode is of 60 mm in diameter is connected to the ground. The voids are of 0.6 mm diameter and 50 μm thickness, created at the center of the middle layer of 7 poly-ethylene-terephthalate (PET) samples. The surface discharge in air was simulated by placing a small brass ball of 55 mm diameter on perspex of geometrical size 65 mm x 65 mm x 8 mm. The surface discharge in oil is simulated by a pressboard embedded in a container with Castrol insulating oil [15]. A needle was placed at a predetermined angle to the surface of the pressboard and 45 mm distance from a block earth electrode, also placed on the pressboard surface[17]. Examples of the ϕ -q-n patterns for several of the considered PD fault geometries are shown in Fig. 2. For corona in air, the positive and negative ϕ -q-n patterns have been separated for improved visibility of the positive corona discharges characterized by their small repetition rate.

Fig 1: Simulated PD faults: a) surface discharge in air, b) single void in PET, c) corona in air and d) surface discharges in oil.

The experimental conditions and test ϕ -q-n samples generated for each PD fault type is shown in Table 1. For each fault, relatively large ϕ -q-n samples were generated so as to determine reliable 95% mean CI limits for improved evaluation by the SNN and ENN. For corona in air, measurements were taken at several voltages over two gap distances of 5mm and 10mm because of the discharge behaviour of the positive corona discharge which have low repetition rate and higher amplitude [18]. They are then combined to form the ϕ -q-n corona set for SNN and ENN evaluation.

Fig.2: Example of the ϕ -q-n patterns for the PD faults considered.

Table 1: PD fault types with the test voltages and corresponding ϕ -q-n samples.

138

139 2.2 Experimental test arrangement

140 The PD measurement process was performed in accordance with the IEC60270 PD
 141 standard[19]. The PD detection system produces a power cycle which is used to synchronize
 142 real time ϕ -q-n patterns and possess functions for automatic data logging these patterns at
 143 different time periods as well as controlling changes in PR and AB sizes. This is important
 144 for the work presented in this paper, as several experiments require longer stressing periods
 145 and data is required to be captured and stored systematically over certain resolution size for
 146 analysis. PD calibration was carried out for PD apparent charge determination.

147 2.3 Choice of statistical fingerprints for PD analysis

148

149 For ϕ -q-n evaluation, statistical fingerprints have been widely applied because of their
 150 capability for well-defined pattern quantification [1,15]. In order to simplify the ϕ -q-n
 151 analysis, statistical fingerprints are usually extracted from 2D plots derived from the ϕ -q-n
 152 patterns. The key 2D distributions of interest are the pulse count $H_n(\phi)$, mean pulse-height
 153 $H_{qn}(\phi)$ and amplitude number $H_n(q)$ plots. These plots are presented in both the positive (+)
 154 and negative half power cycles (-).

155

156 Similar to other literature [4], this paper applies 15 statistical parameters that serve as input
 157 fingerprints for training and testing both the ENN and SNN. These include the skewness (sk)
 158 and kurtosis (ku) of the $H_{qn}(\phi)+$, $H_{qn}(\phi)-$, $H_n(q)+$, $H_n(q)-$, $H_n(\phi)+$ and $H_n(\phi)-$ distributions,
 159 the cross-correlation (cc), discharge factor (Q) and modified cross-correlation (mcc).
 160 Definitions of these statistical parameters are available in [1] and their mathematical
 161 expressions are shown in Table 2. In this table, μ represents the mean value, σ is the standard
 162 deviation, n represents the size of the data and P_j is the probability of the discrete values x_j
 163 and y_j . Q^+_s and Q^-_s represent the sum of discharge magnitudes in the positive and negative
 164 half cycles while N^+_s and N^-_s represent the number of discharges in the positive and negative
 165 half power cycle.

166

167 Table 2: Mathematical expressions of statistical fingerprints

168

169 3. Description of the ENN algorithm

170

An ENN is a learning model comprising a limited number of NNs trained for the same task [20]. The ENN can enhance the generalization performance of the SNN by simply training a number of SNNs and combining their output predictions. Diverse types of ENN architectures have evolved. These include the simplest ENN, The Naive classifier technique, the generalised ENN and the dynamically weighted ensemble method (DEM) [21]. The latter determines the neural network weight at any time the network is estimated and provides the best performance at any instant [21]. The weight is proportional to the certainty of the individual NN prediction and this certainty evaluates how close the output is to any known target value. The prediction of the NN can be regarded to be a probability of any occurrence. For example, assume that $b = f(a)$ is the output of the network and a represents the input variables. If b approaches unity, it is more certain that it belongs to a certain class. When b is close to 0, it is certain that this instance is not in that particular class. The certainty of the NN is computed as follows[10],

$$c(b) = \begin{cases} b & \text{if } b \geq 0.5 \\ 1-b & \text{otherwise} \end{cases} \quad (1)$$

The prediction of the Dynamically Averaged Network (DAN) can be computed as follows:

$$f_{DAN} = \sum_{j=1}^n w_j f_j(a) \quad (2)$$

where the weights w_i are defined based on

$$w_j = \frac{c(f_j(a))}{\sum_{j=1}^n c(f_j(a))}. \quad (3)$$

Figure 3 shows the proposed ENN model for recognition of the PD patterns. The ENN developed in this work comprises several SNN architectures having the same configuration but with different initial parameters. To obtain accurate values of bias and variance [22], the ENN model is trained from bootstrapped resample data. Bootstrap resampling is a criterion employed at the instance when the input fingerprints for the NN are limited. It is implemented so as to have a number of resampled datasets that can be applied as input (i.e. training) fingerprints for several NNs. With this strategy, the resampled datasets have the same dimension as the original dataset in such a way that some samples are replicated while others are discarded. Bootstrap resampling provides an accurate value of the variance and

bias of the NN. This technique has been successfully applied to the ENN of various categories of data in the medical and engineering related fields and has demonstrated improved results [20,21,22].

Fig.3: The ENN model.

Among the various ENN data aggregation techniques, the dynamically weighted ensemble has been shown to outperform others in different application scenarios, e.g. in Ref [23], and therefore as a consequence this paper applies the same techniques to evaluate the SNN outputs in the ensemble. Six SNNs are applied in this work in order to have a reasonable number of diverse models to improve the generalization.

4 PD faults analysis

This section presents the results of statistical fingerprint classification sensitivity to different PR and AB resolution sizes of the $H_{qn}(\varphi)+$, $H_{qn}(\varphi)-$, $H_n(q)+$, $H_n(q)-$, $H_n(\varphi)+$ and $H_n(\varphi)-$ distributions. In evaluating fingerprints for variable PR the $H_n(q)$ distributions have not been considered because they do not demonstrate any statistical variation. This is expected because PR change only affect the phase bins not the amplitude bins. Similarly when evaluating AB, the $H_n(\varphi)$ statistics have not been considered. Additionally, the sensitivity of Q , cc and mcc were not considered, because they are found to be insensitive to different resolution sizes. For Q , the mean discharge level is undoubtedly the same for any φ - q - n resolution changes, while for cc the correlation of the positive and the negative half power cycles remain unchanged for φ - q - n resolution variations.

As an example, the influence of the change in PR and AB sizes on phase and amplitude resolved patterns for surface discharge in air is shown in Fig.4. The φ - q - n patterns were initially captured at 1° PR and 100 AB. Then, two approaches were implemented for data transformation. First, φ - q - n fingerprints were captured at 1° PR and 100 AB over the 360° cycle and transformed to 3°, 6°, 9°, 12° and 15° PR, keeping the AB size constant. Second, based on the transformation of the φ - q - n fingerprint in the first strategy, samples having 6° PR and 100AB are further transformed to 50 AB and 25 AB, keeping the PR size constant. The plots visually show that as the resolution is varied from 1° to 15° or 100 AB to 25 AB, discharge numbers for each PR or AB vary resulting in potentially different statistical

variability of the ϕ -q-n patterns. For reliable statistical evaluation, 95% CI for different PR and AB sizes were obtained over large ϕ -q-n samples as summarised in Table 1. As an example, the 95% statistical CIs for air surface discharges and the dielectric bounded void are presented in the Appendix for different PR and AB sizes.

There are three essential deductions:

1) The sk and ku mean values and CIs of $H_n(q)$ are more sensitive to different PR sizes than AB sizes when compared to that of the sk and ku of other distributions, e.g. $H_n(\phi)$ and $H_{qn}(\phi)$. This is attributed to the $H_n(q)$ distributions becoming increasingly peaked as the AB sizes are reduced.

2) The sk and ku mean values and CIs of the $H_{qn}(\phi)$ appear to show higher sensitivity levels to different PR sizes than AB. As the PR increases, PD patterns become flatter across the phase dimension resulting in statistical changes.

3) The cc is sensitive to different PR and AB sizes, but no defined variation trend is visible across the various geometries considered. This is due to several factors affecting the cc which varies from one PD fault to the other e.g. the discharge amplitude distribution, flatness and peakedness of the distribution.

Fig. 4: Processed surface discharge in air patterns.

5. Application of the ENN to discriminate different PD ϕ -q-n resolutions

5.1 SNN and ENN training and testing approaches

To evaluate the robustness of the SNN and ENN in classifying and discriminating the statistical variations for different PR or AB sizes of the ϕ -q-n patterns, two strategies were implemented:

- 1) Firstly, both the SNN and ENN were trained with the 6° PR, 100 AB captured ϕ -q-n fingerprints and then tested with the same data, but using 3° , 12° and 15° PR and 100 AB. This was to determine the robustness of the SNN and ENN in capturing statistical variations arising from different PR size of the ϕ -q-n patterns.

2) Secondly, the first strategy was repeated except that the testing was carried out with 25AB and 50AB ϕ -q-n data but all at 6° PR. This aims at determining whether the SNN and ENN can still capture statistical variations that may arise from a different AB resolution of the ϕ -q-n patterns.

5.2 Statistical merit indicators for comparing the SNN and ENN recognition rates

As stated in the literature [22], the major weakness of the SNN lies with its various performance evaluation, when trained with several initial conditions (i.e. weights and biases). To improve the situation, this paper applied statistical measures such as the average, variance and standard error of the mean (SEM) for the SNN and ENN comparison[15]. To obtain a certain degree of precision on the classification outcomes and as used in a previous paper, 100 iterations were chosen for all statistical determinations[15]. This aims at developing and comparing statistical error bound recognition efficiencies of the SNN and ENN for the various ϕ -q-n resolution sizes.

5.3 Results and discussion

Similar to previous research work [1,15,24], statistical measures extracted from ϕ -q-n fingerprints at different resolution dimensions form the input fingerprints for SNN and ENN evaluation. To classify and discriminate these extracted statistical features, as a case study, this paper considered surface discharge in air patterns as the training set, while testing was carried out with the same surface discharge data and other PD faults of different PR and AB dimensions. Six generated ϕ -q-n datasets, Data 1 through to Data 6 are shown in Table 3.

Table 3: Samples of training and testing data for the SNN and ENN

Both the SNN and ENN were evaluated using statistical data of **Data 1, Data 2, Data 3, Data 4, Data 5** and **Data 6**. Each set of fingerprints was composed of a matrix of size 28 rows x 17 columns. The first 15 columns were considered to be the input data, while the remaining 2 were the output fingerprints. The input fingerprints into the SNN and ENN are the PD samples shown in Table 3, while the output parameters for the PD sample fault are chosen to be [0 1], [1 0], [0 0] and [1 1]. For each PD fault data matrix, 8 rows out of 28 were selected as the testing fingerprints for the SNN and ENN. The ENN configuration is composed of six networks with the same structure trained and tested from the 28 row vectors of bootstrapped

resampled data. In order to choose the best SNN set-up for the ensemble, the hidden layer, learning and momentum rates were adjusted and optimum parameters chosen for comparison with the SNN with these forming the configurations for the ENN. One hidden layer with 25 neurons was selected, having momentum and learning rates of 0.9 and 0.06 respectively.

Figs. 5, 6, 7 and 8 show the classification performance of the SNN and ENN when **Data 1** is used for training and then testing undertaken with **Data 1, Data 2, Data 3 and Data 4** respectively. Similarly, Figs. 9 and 10 demonstrate the classification result of the SNN and ENN when **Data 1** is used for training and then testing undertaking with **Data 5 and Data 6**. From these figures, the following information have been deduced:

- 1) When either the SNN or ENN is trained and tested with the same PD fault having the same PR and AB size of the ϕ -q-n patterns, the ENN shows improved recognition performance over the SNN (see Fig.5). It is obvious that μ_E , σ_E and σ_{EM} shows higher recognition values than that of μ_S , σ_S and σ_{SM} . For the SNN and ENN trained with one PD fault and test with another, the ENN does not always produce an improved recognition performance over the SNN. This is clearly demonstrated by the σ_E and σ_{EM} having identical recognition intervals to σ_S and σ_{SM} , but still μ_E is greater than μ_S , showing that on average the ENN has an improved recognition result in comparison to the SNN.
- 2) For the SNN and ENN trained with surface discharge in air data of one resolution size and then tested with the same data having different resolution sizes (Figs. 6-10), the ENN and SNN both appear to show higher average recognition probability compared to the other PD faults. However, the ENN appears to be better in this case as its variance intervals are always higher than any other tested PD faults (σ_E and σ_{EM} shows higher recognition values than that of the σ_S and σ_{SM}), indicating the ENN's improved capability to recognize closely similar PD statistical fingerprints. This result implies that even with a change in resolution sizes, it is possible to determine closely similar PD fault scenarios using the SNN and the ENN.
- 3) To examine the capabilities of the SNN and ENN in relation to two PR sizes of the ϕ -q-n patterns Figs. 5-8 were evaluated. The most visible change is between Figs. 5 and 8 i.e. when the resolution size is changed from 6° to 15°, whilst there is insignificant change in the SNN and ENN recognition capabilities when the resolution size is

changed from 6° to 12° or from 6° to 3° . There is basically very little decrease in the values of μ_S and μ_E that can be statistically quantified. Comparing Figs. 5 and 8 shows that there is a slight decrease in the values of μ_S and μ_E in Fig.8 compared to that of Fig.5, which appears not to be statistically significant. Generally, there is rise in the values of μ_S , μ_E , σ_E , σ_S , σ_{EM} and σ_{SM} for untrained PD faults in Fig.8 when compared to these parameters in Fig. 5, but the ENN parameters clearly show a rise in the statistical indicators compared to the SNN. This result implies that the ENN appears to be more sensitive in discriminating the 2 PRs of the ϕ -q-n patterns, however there exists little variation in the 2 PR ϕ -q-n patterns applied for training and testing both the ENN and SNN.

- 4) To examine the performance of the SNN and ENN in capturing two AB sizes of the ϕ -q-n patterns, Figs. 9, 10 and 5 were compared. Generally, lower values of μ_S and μ_E are visible for surface discharge in air (when compared to training and testing surface discharge in air at the same resolutions or 2 PRs of the ϕ -q-n patterns i.e. Figs. 5-8). The change appears to be more visible in the SNN and ENN recognition rates when the AB resolution size is changed from 100AB to 25AB rather than 50AB. For both changes there is at least a 5% reduction in the recognition rates of the SNN and ENN for surface discharge in air. However, when the resolution size is changed from 100AB to 25AB it is obvious that σ_E , σ_S , σ_{EM} , σ_{SM} values of Fig. 10 appear to be higher than those of Fig. 5 and Fig. 9. This shows a much wider correlation exists of the testing data with the training data. Comparing Fig. 10 and Fig. 5 shows that the ENN has higher sensitivity in statistical operator variations compared to the SNN. This results implies that there exists significant variations between the training and testing data caused by the change in the AB size of the ϕ -q-n patterns.

Fig. 5. Plot of μ_S , μ_E , σ_S , σ_E , σ_{SM} and σ_{EM} when both SNN and ENN are trained with surface discharge in air 6° PR and 100 AB and tested with the same surface discharge and 3 other PD faults but at 6° PR and 100 AB. (μ_S and μ_E values are the centre of variances of SNN and ENN).

Fig. 6. Plot of μ_S , μ_E , σ_S , σ_E , σ_{SM} and σ_{EM} when both SNN and ENN are trained with surface discharge in air 6° PR and 100 AB and tested with the same surface discharge and 3 other PD faults but at 3° PR and 100 AB μ_S and μ_E values are the centre of variances of SNN and ENN).

Fig. 7. Plot of μ_S , μ_E , σ_S , σ_E , σ_{SM} and σ_{EM} when both SNN and ENN are trained with surface discharge in air 6° PR and 100 AB and tested with the same surface discharge and 3

other PD faults but at 12° PR and 100 AB (μ_S and μ_E values are the centre of variances of SNN and ENN).

Fig. 8 Plot of μ_S , μ_E , σ_S , σ_E , σ_{SM} and σ_{EM} when both SNN and ENN are trained with surface discharge in air 6° PR and 100 AB and tested with the same surface discharge and 3 other PD faults but at 15° PR and 100 AB (μ_S and μ_E values are the centre of variances of SNN and ENN).

Fig. 9 Plot of μ_S , μ_E , σ_S , σ_E , σ_{SM} and σ_{EM} when both SNN and ENN are trained with surface discharge in air 6° PR and 100 AB and tested with the same surface discharge and 3 other PD faults but at 6° PR and 50 AB (μ_S and μ_E values are the centre of variances of SNN and ENN).

Fig. 10 Plot of μ_S , μ_E , σ_S , σ_E , σ_{SM} and σ_{EM} when both SNN and ENN are trained with surface discharge in air 6° PR and 100 AB and tested with the same surface discharge and 3 other PD faults but at 6° PR and 25 AB (μ_S and μ_E values are the centre of variances of SNN and ENN).

6. Conclusions

For the majority of the PD sources considered, statistical mean CI variations exist for different PR and AB sizes. This has been shown to be most significant in the $H_n(q)+$ and $H_{qn}(\varphi)-$ plots but less significant in the $H_n(\varphi)$ plots. Both the SNN and ENN capabilities have been tested for recognizing and discriminating resolution sizes of the φ -q-n patterns and the results clearly show that they can detect slight changes in resolution sizes of these patterns. Additionally, the results shows that the ENN, being more capable, is more sensitive in capturing several resolution changes. These results imply that for practical PD recognition applications, care has to be taken not to simply train SNN or ENN with any PD φ -q-n resolution data and test with another φ -q-n resolution data and expect to obtain reliable results. Furthermore, since different measuring instruments may have different settings for the φ -q-n patterns which are captured and stored for analysis, it is important that certain φ -q-n PR and AB sizes be maintained for consistency of recognition, otherwise unreliable predictions may be incurred.

Acknowledgment

The authors are grateful to the Petroleum Technology Development Fund, Nigeria for providing financial support.

References

- 1) E. Gulski and A. Krivda, Neural Network as a tool for recognition of partial discharges, IEEE Trans. on Electrical Insulation. 28(6) (1993) 984-1001.
- 2) CIGRE, Working group report 21.03. Recognition of discharges. Electra 11(1969) 61–98.
- 3) A. Krivda, Automated recognition of partial discharges, IEEE Trans. on Dielectrics and Electrical Insulation. 2(5) (1995) 792-821.
- 4) J. Granadoa, C. Álvarez-Arroyo, A. Torralbaa, J.A. Rosendo-Macias, A. Chávez, M. Burgos-Payánb, Time domain analysis of partial discharges envelope in medium voltage XLPE cables, Electric Power System Research. 125 (2015) 220-227.
- 5) R. Albarracín, J.A. Ardila-Rey and A. Abubakar Mas'ud, On the use of monopole antennas for determining the effect of the enclosure of a power transformer tank in partial discharges electromagnetic propagation, Sensors. 16(2) (2016) 148.
- 6) Y. Tu, Z. Wang, and P. Crossley, Partial discharge pattern recognition based on 2D wavelet transform and neural networks techniques. Power Engineering Society SUMMER Meetings 1(2002) 411-416.
- 7) M. Majidi, M.S. Fadali, M. Etezadi-Amoli and M. Oskuoee, Partial discharge pattern recognition via sparse representation and artificial neural network, IEEE Transactions on Dielectrics and Electrical Insulation. 22(2) (2015) 1061-1070.
- 8) E. Gulski, F. Krueger, Computer aided analysis of discharge patterns, Journal of Applied Physics. 23(1990) 1569-1575.
- 9) W. J. K. Raymond, H. A. Illias, A. H. A. Bakar and H. Mokhlis, Partial discharge classifications: review of recent progress, Measurement. 68 (2015) 164-181.
- 10) T. Abdel Galil, R. Sharkawy and M. Salama, Partial discharge pattern classification using the fuzzy decision tree approach, IEEE Trans on Instrumentation and Measurement. 54(6) (2005) 2258-2263.
- 11) T. Babnik, R. Aggarwal, and P. Moore, Data mining on a transformer partial discharge data using the self-organizing map, IEEE Transactions on Dielectrics and Electrical Insulation. 14(2) (2007) 444-452.
- 12) Y. Khan, A. Khan, F.N. Budimana, A. Beroual, N. H. Malika and A. A. Al-Arainya. Partial discharge pattern analysis using support vector machine to estimate size and position of metallic particle adhering to spacer in GIS, Electric Power System Research. 116 (2014) 391-398.
- 13) T. K. Abdel-Galil, Y. G. Hegazy, M. M. A. Salama and R. Bartnikas, Partial discharge pulse pattern recognition using hidden Markov models, IEEE Transactions on Dielectrics and Electrical Insulation. 11 (4) (2004) 715-723.
- 14) B. Karthikeyan, S. Gopal and S. Venkatesh, ART 2—an unsupervised neural network for PD pattern recognition and classification, Expert Systems with Applications. 31(2) (2006) 345-350.

- 15) A. Abubakar Mas'ud, B. G. Stewart, S. G. McMeekin, Application of Ensemble neural networks for classifying partial discharge patterns, *Electric power system research*. 110 (2014) 154-162.
- 16) C. Kuo, Artificial identification system for transformer insulation aging, *Expert Systems with Applications*. 37(6) (2010) 4190-4197.
- 17) A. Abubakar Mas'ud, B. G. Stewart, S. G. McMeekin and A. Nesbitt, Partial discharge pattern classification for angled point-oil-pressboard degradation, *IEEE Conference of Electrical Insulation and Dielectric Phenomena*. (2013) 217-220.
- 18) N. Trinh, Partial discharge XIX: Discharges in air Part I: Physical mechanisms, *IEEE Insulation Magazine*. 11(2) (1999) 23-29.
- 19) IEC 60270, British standard guide for partial discharge measurement (2001).
- 20) I. Maqsood, M. Khan and A. Abraham, An ensemble of NNs for weather forecasting, *Neural Computing and Application*. 13 (2004) 112-122.
- 21) D. Jiminez, Dynamically weighted ensemble of neural network for classification, *World Congress on Computational Intelligence*. (1998) 753-756.
- 22) P. Cunningham, J. Carna and S. Jacob, Stability Problems with the artificial neural networks and the ensemble Solution, *Art. Intelligence in Medicine*. 20(3) (2000) 217-225.
- 23) H. Navone, P. Grannito, P. Verdes, H. Ceccato, A learning algorithm for NN ensemble, *Artificial Intelligence*. 12 (2001) 70-74.
- 24) M. Majidi, M. Oskuoee, Improving pattern recognition accuracy of partial discharges by new data preprocessing methods, *Electric power system research*. 119 (2015) 100-110.

Figures

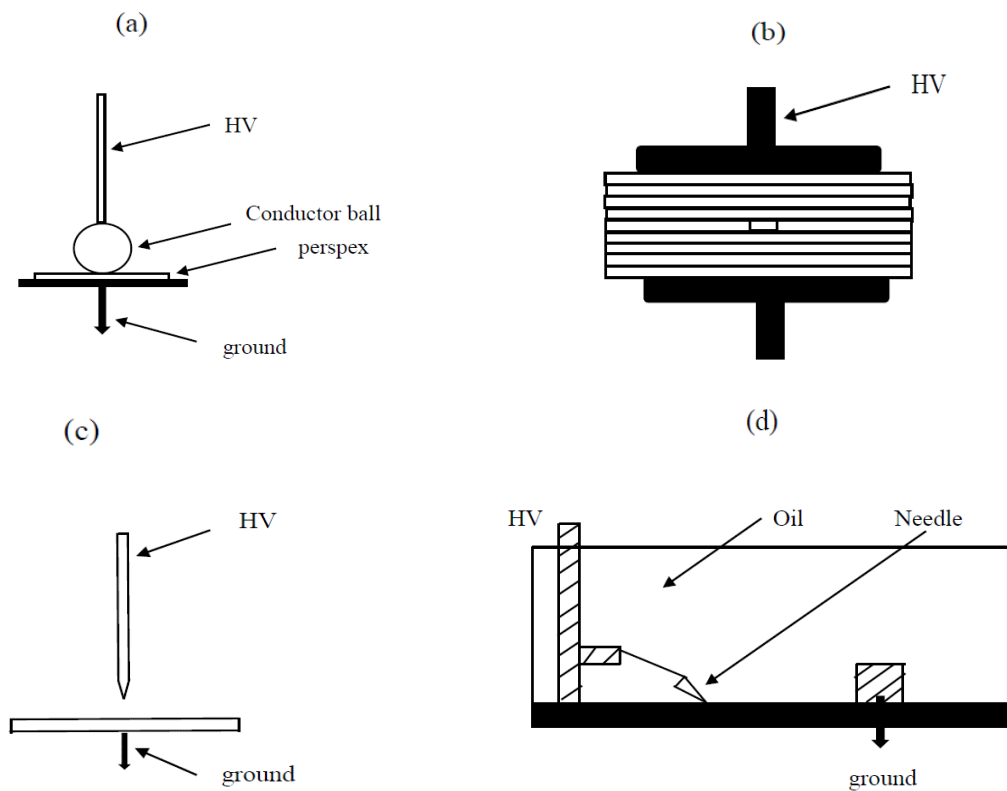
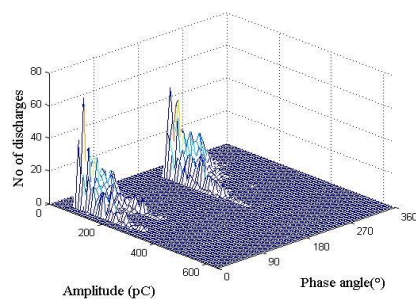
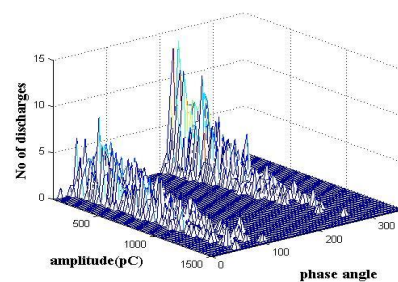


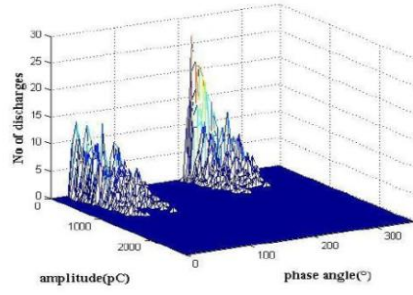
Fig. 1: Simulated PD faults a) surface discharge in air b) single void in PET c) corona in air d) surface discharges in oil



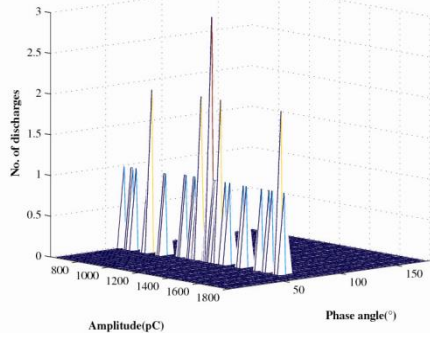
(a) Single void



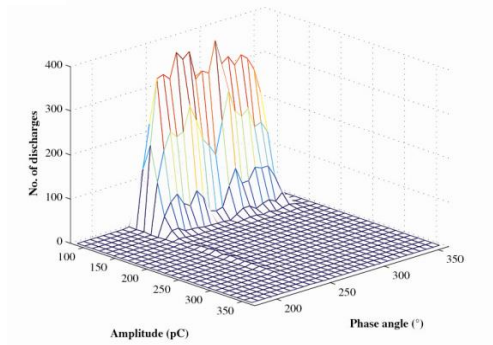
(b) surface discharge in air



(c) surface discharge in oil



(d) +ve corona in air



(e) -ve corona in air

Fig. 2: Example of the ϕ -q-n patterns for the PD faults considered

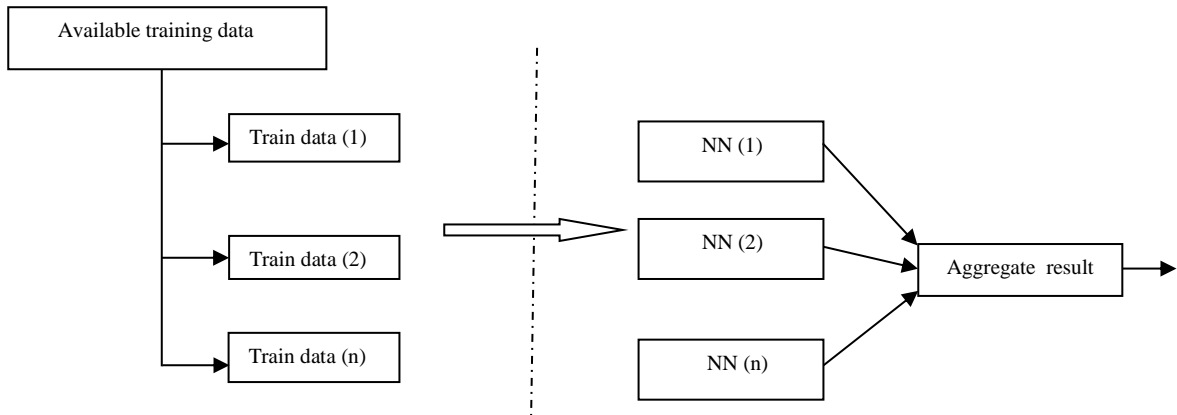
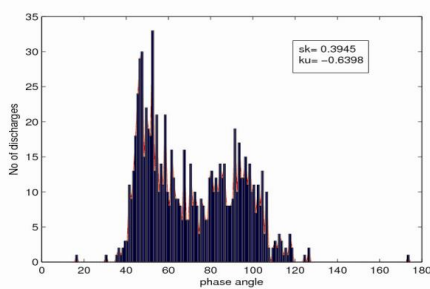
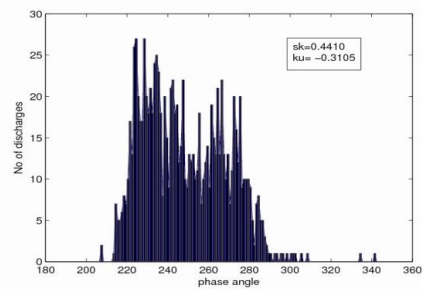


Fig. 3: The ENN model[10]

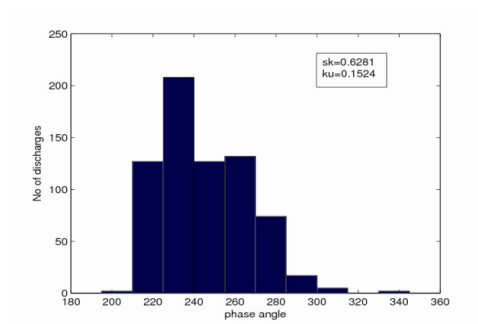
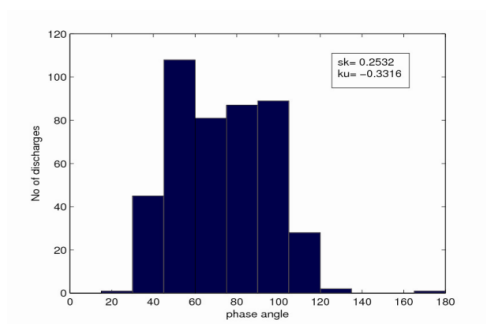


$H_n(\phi)^+$ at 1°PR and 100 AB



$H_n(\phi)^-$ at 1°PR and 100 AB

550

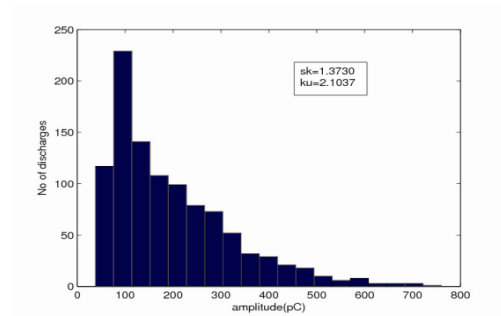
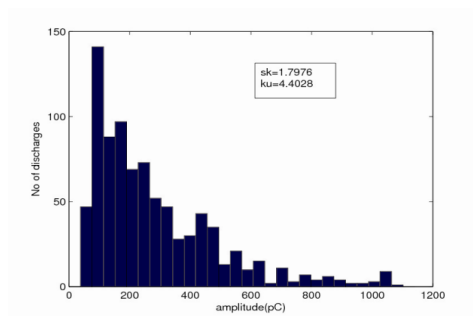


551

552

$H_n(\varphi)+$ at 15°PR and 100 AB

$H_n(\varphi)-$ at 15°PR and 100 AB

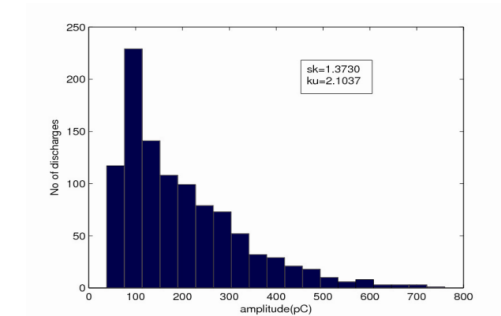
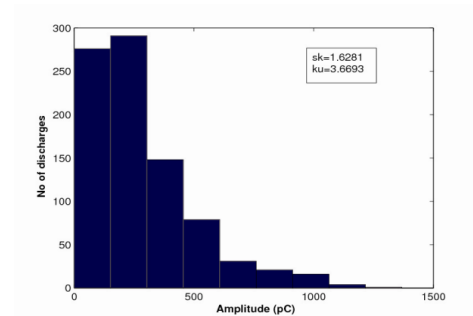


553

554

$H_n(q)-$ at 6°PR and 100 AB

$H_n(q)-$ at 6°PR and 100 AB



555

556

$H_n(q)+$ at 6°PR and 25 AB

$H_n(q)+$ at 6°PR and 25 AB

557

Fig. 4: Processed surface discharge in air patterns.

558

559

560

561

562

563

564

565

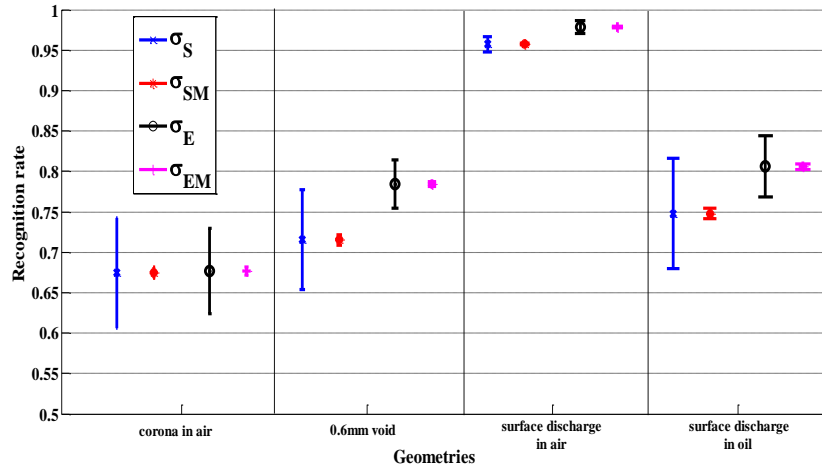


Fig. 5. Plot of μ_S , μ_E , σ_S , σ_E , σ_{SM} and σ_{EM} when both SNN and ENN are trained with surface discharge in air 6° PR and 100 AB and tested with the same surface discharge and 3 other PD faults but at 6° PR and 100 AB. (μ_S and μ_E values are the centre of variances of SNN and ENN)

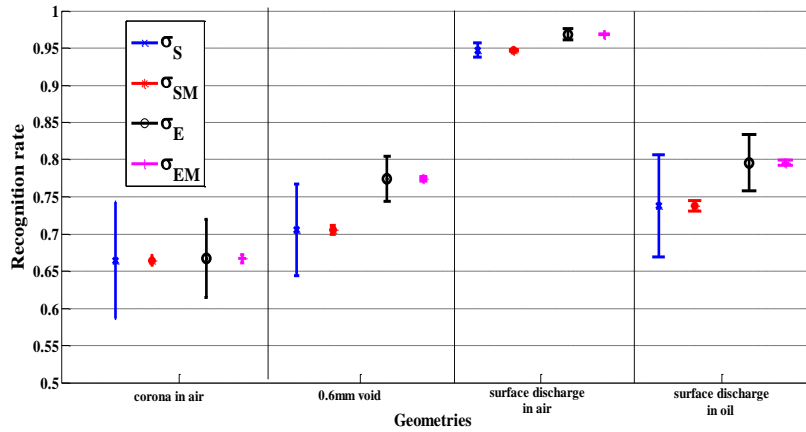


Fig. 6. Plot of μ_S , μ_E , σ_S , σ_E , σ_{SM} and σ_{EM} when both SNN and ENN are trained with surface discharge in air 3° PR and 100 AB and tested with the same surface discharge and 3 other PD faults but at 3° PR and 100 AB (μ_S and μ_E values are the centre of variances of SNN and ENN)

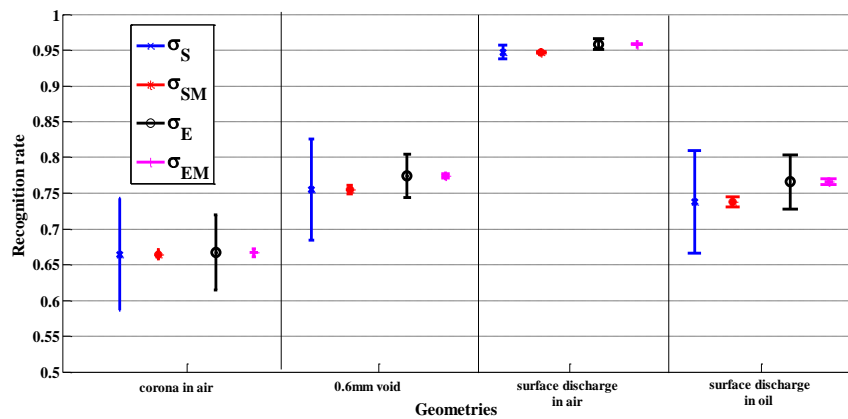


Fig. 7. Plot of μ_S , μ_E , σ_S , σ_E , σ_{SM} and σ_{EM} when both SNN and ENN are trained with surface discharge in air 12° PR and 100 AB and tested with the same surface discharge and 3 other PD faults but at 12° PR and 100 AB (μ_S and μ_E values are the centre of variances of SNN and ENN)

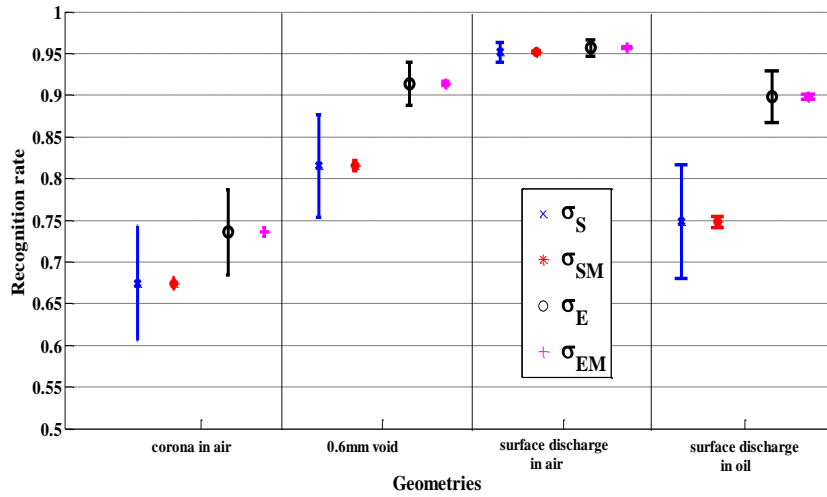


Fig. 8 Plot of μ_S , μ_E , σ_S , σ_E , σ_{SM} and σ_{EM} when both SNN and ENN are trained with surface discharge in air 6° PR and 100 AB and tested with the same surface discharge and 3 other PD faults but at 15° PR and 100 AB (μ_S and μ_E values are the centre of variances of SNN and ENN)

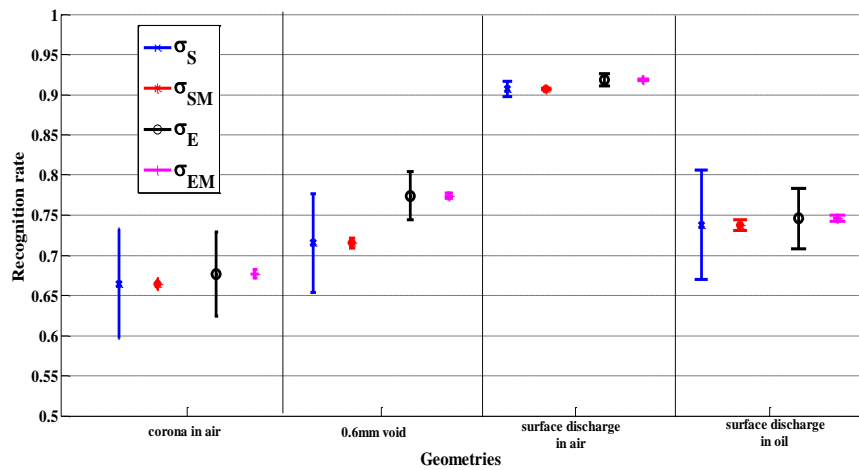
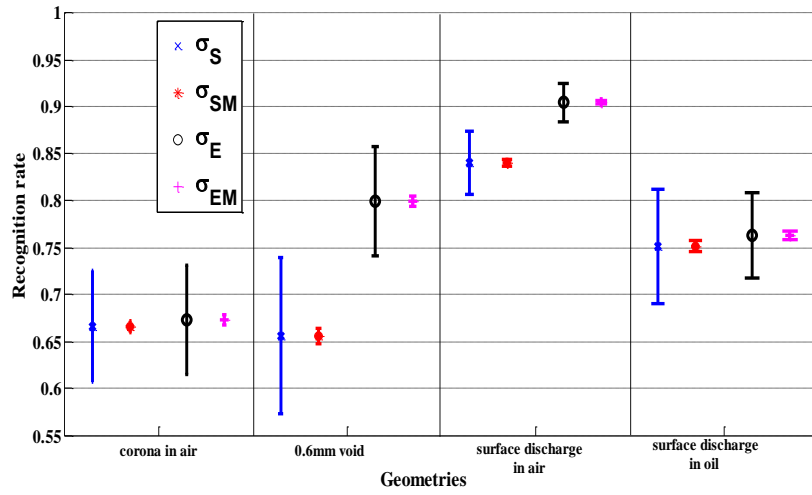
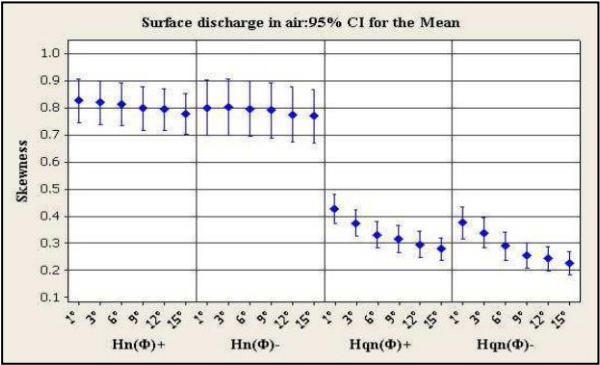


Fig. 9 Plot of μ_S , μ_E , σ_S , σ_E , σ_{SM} and σ_{EM} when both SNN and ENN are trained with surface discharge in air 6° PR and 100 AB and tested with the same surface discharge and 3 other PD faults but at 6° PR and 50 AB (μ_S and μ_E values are the centre of variances of SNN and ENN)

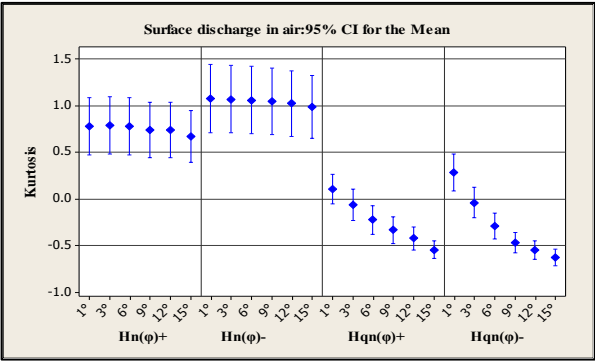


589

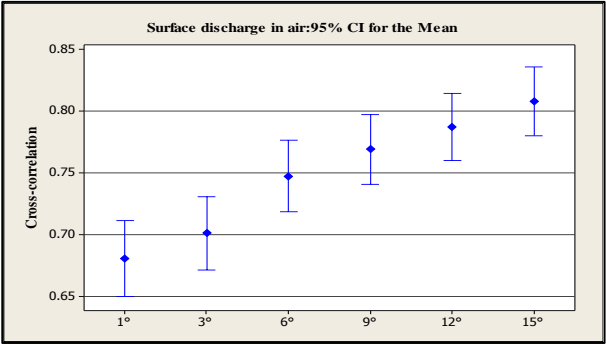
590 Fig. 10 Plot of μ_S , μ_E , σ_S , σ_E , σ_{SM} and σ_{EM} when both SNN and ENN are trained with surface discharge in air
591 6° PR and 100 AB and tested with the same surface discharge and 3 other PD faults but at 6° PR and 25 AB (μ_S
592 and μ_E values are the centre of variances of SNN and ENN)



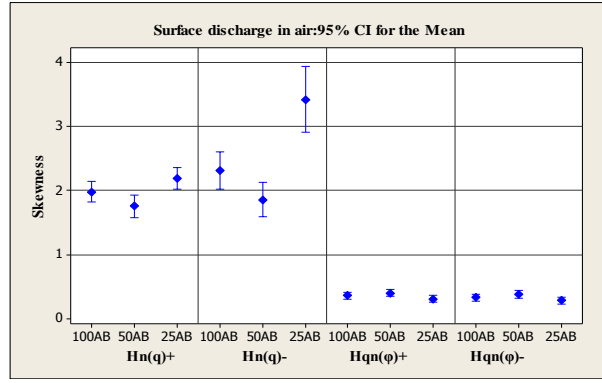
a) *sk* of the 1°, 3°, 6°, 9°, 12° and 15° PR for the $H_n(\varphi)$ and $H_{qn}(\varphi)$ plots at 100 AB



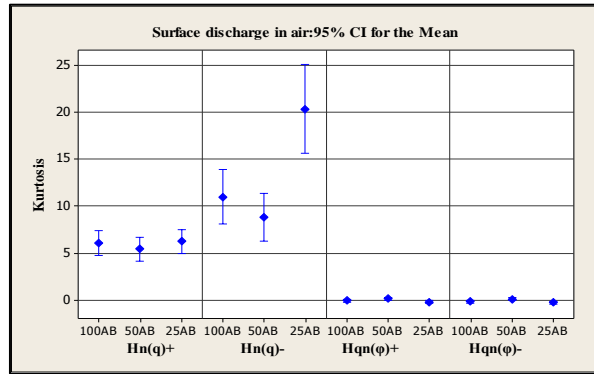
b) *ku* of 1°, 3°, 6°, 9°, 12° and 15° for the $H_n(\varphi)$ and $H_{qn}(\varphi)$ plots at 100 AB



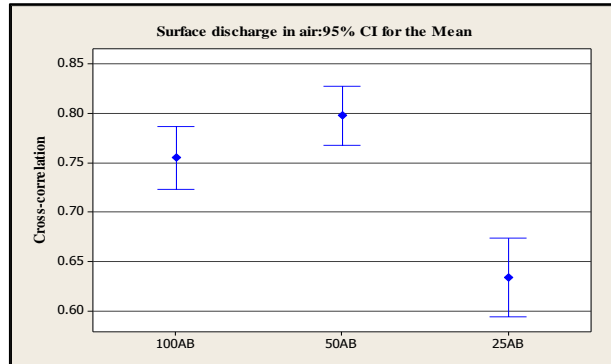
c) *cc* of 1°, 3°, 6°, 9°, 12° and 15° PR for the $H_n(\varphi)$ and $H_{qn}(\varphi)$ plots at 100 AB



d) *sk* of the 100AB, 50AB and 25AB PR for $H_n(q)$ and $H_{qn}(\phi)$ plots at 6° PR

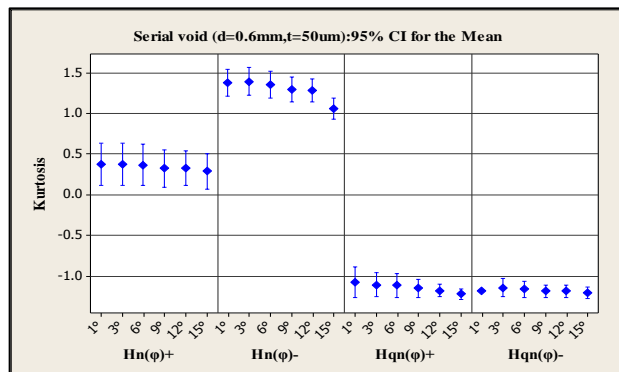


e) *ku* of the 100AB, 50AB and 25AB PR for $H_n(q)$ and $H_{qn}(\phi)$ plots at 6° PR



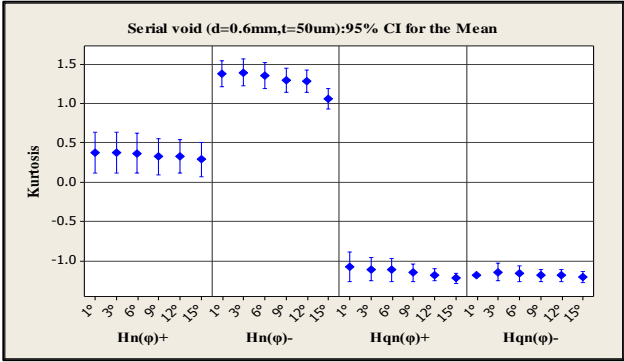
f) *cc* of 100AB, 50AB and 25AB data all at 6° PR.

Fig. A1: The mean values and 95% CI of the mean for surface discharge in air



a) *sk* of the 1° , 3° , 6° , 9° , 12° and 15° PR for the $H_n(\phi)$ and $H_{qn}(\phi)$ plots at 100 AB

620

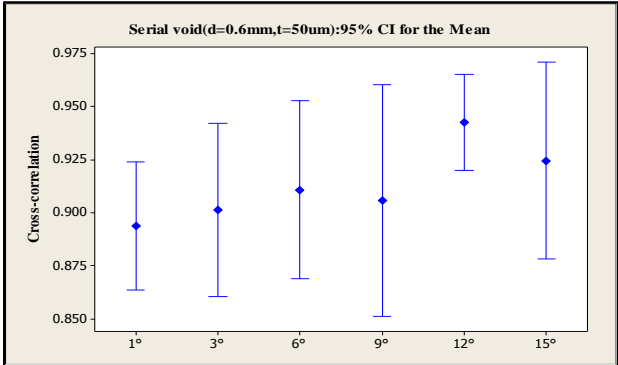


621

622

623

b) ku of the $1^\circ, 3^\circ, 6^\circ, 9^\circ, 12^\circ$ and 15° PR for the $H_n(\varphi)$ and $H_{qn}(\varphi)$ plots at 100 AB

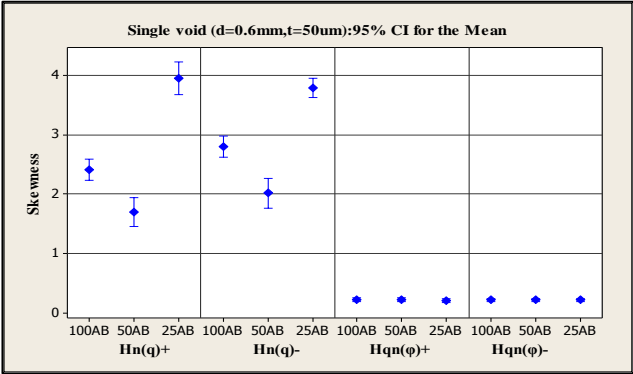


624

625

626

c) cc of $1^\circ, 3^\circ, 6^\circ, 9^\circ, 12^\circ$ and 15° PR for the $H_n(\varphi)$ and $H_{qn}(\varphi)$ plots at 100 AB



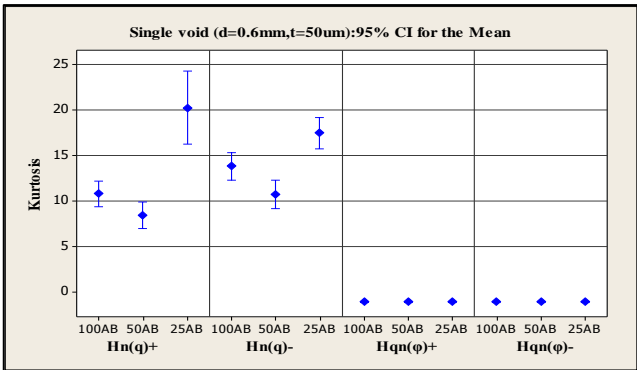
627

628

629

630

d) sk of the 100AB, 50AB and 25AB PR for $H_n(q)$ and $H_{qn}(\varphi)$ plots at 6° PR

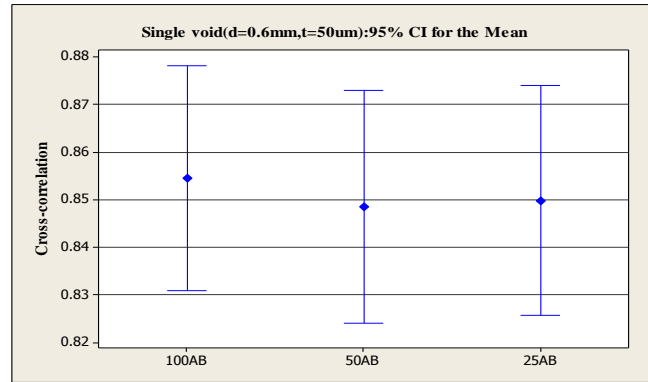


631

632

633

e) sk of the 100AB, 50AB and 25AB PR for $H_n(q)$ and $H_{qn}(\varphi)$ plots at 6° PR



f) *cc* of 100AB, 50AB and 25AB data all at 6° PR.

Fig. A2: The mean values and 95% CI of the mean for single void in PET

Tables:

Table 1: PD fault types with the test voltages and corresponding ϕ -q-n samples.

PD fault type	Test voltage	ϕ -q-n samples generated
Corona in air	1.5 kV, 1.9 kV, 2 kV and 2.2 kV for the 5 mm gap and 1.7 kV, 1.9 kV, 2.3 kV and 2.8 kV for the 10 mm gap distance	42
Surface discharge in air	5 kV	148
Surface discharge in oil	18.5 kV	90
Void in the insulation	2.7 kV	169

657

Table 2: Mathematical expressions of statistical fingerprints

Statistical operator	Mathematical equation
Skewness	$sk = \frac{\sum (x_j - \mu)^3 P_j}{\sigma^3}$
Kurtosis	$ku = \frac{\sum (x_j - \mu)^4 P_j}{\sigma^4}$
Discharge Factor	$Q = \frac{Q_s^- / N_s^-}{Q_s^+ / N_s^+}$
Cross-correlation	$cc = \frac{\sum x_j y_j - \frac{\sum x_j \sum y_j}{n}}{\sqrt{\left[\sum x_j^2 - \frac{(\sum x_j)^2}{n} \right] \left[\sum y_j^2 - \frac{(\sum y_j)^2}{n} \right]}}$

658

659

660

661

Table 3: Samples of training and testing data for the SNN and ENN

Samples	Description
Data 1	surface discharge in air ϕ -q-n data at 6° PR and 100 AB
Data 2	surface discharge in air and 3 other PD faults ϕ -q-n data, all at 3° PR and 100AB
Data 3	surface discharge in air and 3 other PD faults ϕ -q-n data, all at 12° PR and 100AB
Data 4	surface discharge in air and 3 other PD faults ϕ -q-n data, all at 15° PR and 100AB
Data 5	surface discharge in air and 3 other PD faults ϕ -q-n data, all at 6° PR and 50 AB.
Data 6	surface discharge in air and 3 other PD faults ϕ -q-n data, all at 6° PR and 25 AB.

662

663